Sediment Transport Analysis in Manoligao Watershed, Cagdianao, Dinagat Islands, Philippines

Jermelyn C. Laroa
Department of Geology, Caraga State University

Chrester Lou R. Ocay
Department of Geology, Caraga State University

Yvonne T. Olayvar
Department of Geology, Caraga State University

Arnaldo C. Gagula
Caraga Center for Geo-Informatics (CCGeo), College of Engineering and Geosciences, Caraga State University

他

https://doi.org/10.5109/7395520

出版情報：Proceedings of International Exchange and Innovation Conference on Engineering & Sciences (IEICES). 11, pp.212-219, 2025-10-30. International Exchange and Innovation Conference on Engineering & Sciences
バージョン：

Sediment Transport Analysis in Manoligao Watershed, Cagdianao, Dinagat Islands, Philippines

Jermelyn C. Laroa [1], Chrester Lou R. Ocay[1], Yvonne T. Olayvar [1,2,*], Arnaldo C. Gagula [2], Nichole Anthony D. Pacle [1,2]
[1]Department of Geology, [2]Caraga Center for Geo-Informatics (CCGeo), College of Engineering and Geosciences, Caraga State University, Butuan City 8600, Philippines
*Corresponding author email: ytolayvar@carsu.edu.ph

Abstract: *Understanding sediment movement is vital for effective watershed management and sustainable land use planning. This study evaluates sediment transport in the Manoligao Watershed, where sediment particles range from sand to gravel and average water velocity is 0.3148 m/s, varying from 0.0632 to 0.6625 m/s. The lack of fine sediment fractions (<0.075 mm) indicates a crystalline, ultramafic source. Evidence of sediment rounding points to abrasion during transport, while poor sorting, extreme kurtosis, and positive skewness signal fluctuating transport energy and episodic low-energy deposition. The characteristics of the river, such as its narrow shape and cut banks (e.g., SP2, SP4), as well as its extensive joint structures, contribute to this process. In contrast, deposition is linked to low-flow conditions, wider river channels, low sediment yield, and corresponds with the river's morphology (i.e., point bar) (e.g., SP1, SP3). These findings provide a baseline for watershed management and infrastructure planning.*

Keywords: sediment transport, erosion, sediment deposition, watershed management, Dinagat Islands

1. INTRODUCTION

Rivers are extensive natural waterways located in various geographical regions around the world. They consistently flow and significantly impact landscape shaping through erosion and sediment deposition processes [1]. The erosion process concludes when particles are removed from the transporting medium and settle, which is known as deposition [2]. The deposition rate is influenced by the particle's size, shape, and density; generally, more spherical and denser materials settle more quickly.

Erosion is influenced by two main factors: the amount of detached soil and the ability of wind or water to transport that soil. As both detachment and transport require energy, while deposition happens when that energy is no longer available, the erosion process relies on two critical concepts: erosivity, which refers to the energy of the eroding agent (such as wind or water), and erodibility, which denotes the soil's susceptibility to erosion [3].

The Philippines, located in the Pacific typhoon belt, experiences around 20 typhoons annually, which bring intense winds and heavy rainfall. These storms significantly contribute to soil formation through weathering and erosion [4]. Specifically, the Dinagat Islands in southern Philippines have a Type II climate characterized by no dry season. The Philippine Climate Change Commission (PCCC) highlights the challenges posed by soil erosion in a nation highly susceptible to the effects of typhoons. This vulnerability shows the critical need for a thorough understanding of weathering and erosion processes to promote sustainable land and water management practices [3,5].

This baseline study on sediment transport provides essential insight into the river's natural characteristics, especially given the lack of prior research in Dinagat Island, particularly within the Manoligao watershed.

Thus, the study filled this gap by identifying areas of erosion and deposition and examining sediment characteristics and river flow throughout the watershed. Additionally, the findings provide valuable insights that support the development of comprehensive strategies to preserve the watershed and mitigate potential damage.

1.1 Study Area

The Manoligao Watershed, covering an area of 25 km², is one of the largest watersheds on Dinagat Island (Fig. 1). It serves as an essential water source for local communities, supporting both agricultural and domestic needs. Additionally, it is the primary tributary for the Municipality of San Jose, Dinagat, and Basilisa, and holds potential as a source of potable water.

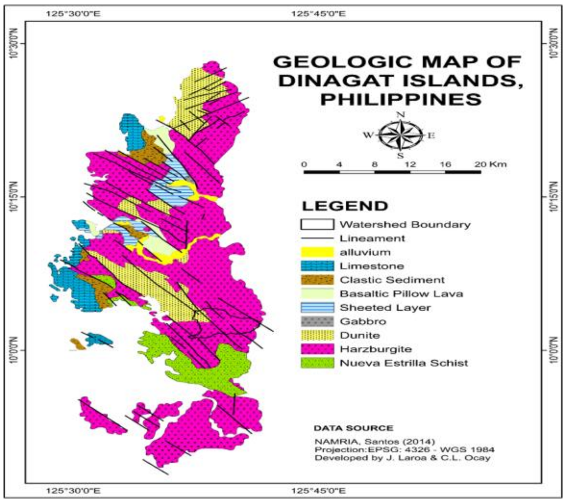

Fig 1. Geologic Map of the Province of Dinagat Island, Mindanao, Philippines.

The watershed is composed of ultramafic terrain, characterized by rocks that are resistant to erosion, as observed in field studies and sediment analysis (Fig. 1). This resistance is attributed to the dense, compact nature of ultramafic minerals (i.e., olivine and pyroxene). However, geologically, these rocks are unstable at the Earth's surface; when exposed to surface conditions, ultramafic minerals undergo rapid chemical weathering, primarily driven by reactions with water and atmospheric CO_2. The continuous movement of water also exerts mechanical forces that fragment and disaggregate the already chemically weakened ultramafic rocks. Hydraulic action, abrasion, and plucking further enhance sediment transport and deposition along the stream courses. In the northern part of the region, there is a significant presence of harzburgite, along with a small amount of dunite.

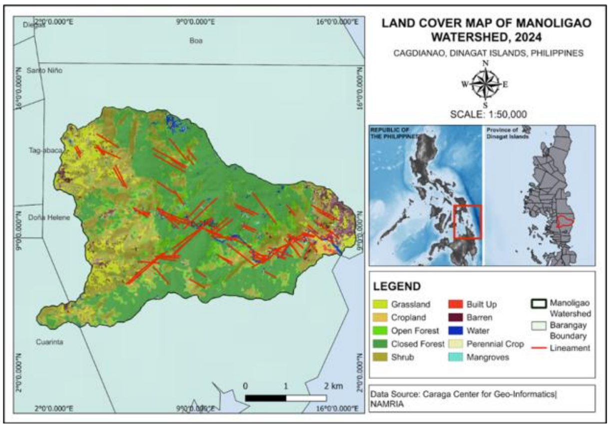

Fig 2. 2024 Land cover map of the Manoligao watershed, created using Google Earth Engine.

Land Cover data shows land use types (e.g., forests, urban areas, croplands) that influence erosion differently. Forests reduce erosion via root stabilization, while impervious urban surfaces increase runoff and erosion risk [6,7]. Combining DEM and land cover data helps pinpoint high-risk erosion zones, enabling targeted conservation efforts. The land cover of the study area is predominantly closed forest (44%) and shrub (31%) (Fig. 2). Furthermore, the area is noted for its highly jointed geological formations.

2. METHODOLOGY

2.1 Fieldwork Approach

This methodology illustrated in Fig 3, involves manual delineation and mapping of erosion and deposition areas along riverbanks and networks to locate the sampling points. Sediment and water samples are collected to analyze the bedload and suspended sediments. To measure the flow velocity that is essential for sediment calculations, a digital water velocity meter is used.

2.1.1 Sediment Characterization

Grain size analysis was conducted using the sieve method with sieves ranging from 3" to No. 200, following ASTM E11 standards. GRADISTAT software was used to characterize sediment distribution and visualize particle size through semi-logarithmic charts and histograms [8].

2.1.2 Total Suspended Sediment (TSS)

TSS is used to calculate the erosion rate. It has different sampling methods. A water sample is needed to acquire the suspended sediment concentration. In the field, a 500 ml clean water bottle is used for the sampling. The sample should be stored at a cool temperature if you need to transport it before laboratory analysis. Then, it is measured in the laboratory by filtering the samples.

2.2 Statistical Analysis

2.2.1 Flow Velocity Calculation

For convenience in converting to cubic feet per second (CFS) flow rate, the formula for calculations in feet and seconds is expressed in equation 1, as follows:

CFS = A × V (area multiplied by velocity) Eq. 1

A (Area) = Width of Channel (feet) × Depth of Water (feet)

V (Velocity) = Distance Traveled/Time to travel (feet traveled divided by seconds)

Discharge = area × velocity

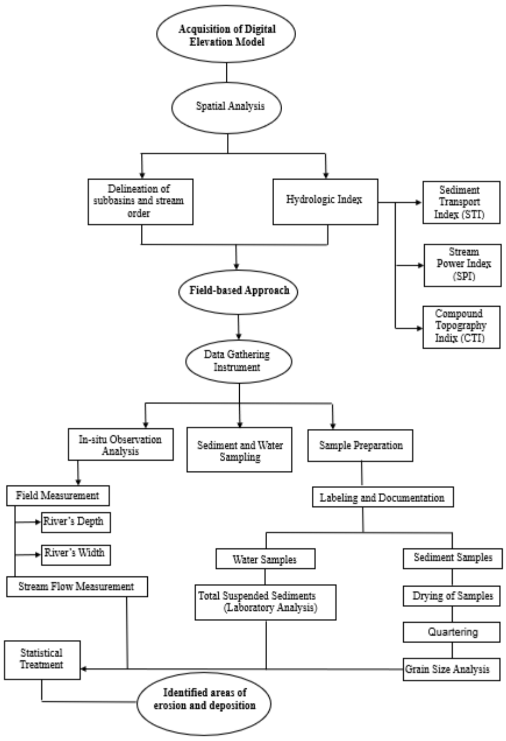

Fig 3. Methodological framework of the study.

2.2.2 Moments Method

Kurtosis and skewness are complementary statistical measures that characterize sediment texture and transport dynamics [9]. The relative importance of the distribution's tails determines the skewness or asymmetry. Positive skewness indicates dominance of finer grains (i.e., the tail is on the right side of the distribution), suggesting transport by suspension or low-energy currents. Negative skewness implies coarser grains (i.e., the tail is on the left side of the distribution), hinting at transport by rolling or bedload in high-energy environments. Kurtosis indicates the sorting efficiency (peakedness of grain-size distribution); the increasing values signify well-sorted sediments, and the decreasing values suggest poorly sorted sediments.

2.2.3 Sediment Budget

The balance between input and output is known as the sediment budget [10], and the river network's erosion rate (ER) in the watershed is quantified. Suspended sediment concentration (SSC) that is measured as mg L^{-1} is calculated using equation 2 as shown below:

$$SSC = W_r - Wf / V \qquad \text{Eq. 2}$$

W_r: Weight of the filtered and dried residue in milligrams
Wf: Weight of the filter in milligrams
V: Sample volume in liters

From SSC, the suspended sediment load (SSL) and suspended sediment yield (SSY) are calculated. The SSL is the sediment carried by the action of water, remaining in suspension. At the same time, the SSY is the total quantified sediment that a river or stream transports at a specific point over a certain period. The formula is SSL= Q (Discharge) × SSC to determine the SSL. After that, the SSY is calculated as SSY= SSL / A (sub-basin catchment area). Then, the sediment budget is calculated and obtained through a mass balance approach by δS = O - I, where δS is the change in storage, O is the sediment output or the SSL in a given station, I is the sediment input or the SSL at the contributing station(s) immediately upstream of it [11]. A positive δS value signifies erosion, whereas a negative δS value indicates deposition. The values for δS, O, and I are measured in volume or mass over the specified period. The erosion rate (ER) is determined using the formula ER = SSY × ρ, where ρ represents the soil density in the watershed.

2.3 Plotting in Hjulstrom Diagram

It describes the relationship between stream flow velocity and particle erosion, transport, and deposition. The erosion velocity curve is represented as a thick line, given that erosion particles are subject to various factors that differ from stream to stream. The graph indicates that transporting particles requires lower flow velocities than erosion, particularly for silt and clay particles. Lastly, the line labelled '*settling velocity*' demonstrates the velocity at which certain-sized particles detach from the transport and deposit [2].

2.4 Spatial Analysis

The delineation of sub-basins and stream order involves key processes such as sink filling to remove terrain pits, calculating flow direction and flow accumulation, and setting a stream threshold to define the stream network. Stream order mapping utilizes a Digital Elevation Model (DEM) to compute flow direction and accumulation, which is then used to establish the stream network. The Strahler method is applied, assigning orders to streams where the smallest tributaries are marked as first-order, and higher orders are incremented when streams of equal order converge.

The study also explores hydrologic indices, which quantify erosion and deposition potential within a watershed based on topographic influence. Derived from DEM data, STI is calculated by: $STI = (m + 1) \times (As / 22.13)^m \times \sin(\beta / 0.0896)^n$, combining the upslope contributing area (As) and local slope gradient (β), using predefined exponents (m = 0.4 and n = 1.3). The Stream Power Index (SPI) measures the erosive power of a river channel. Areas with positive SPI values are associated with higher erosion potential, while negative or lower values suggest zones more favorable for sediment deposition. It is computed using the formula: SPI = ln(Flow Accumulation + 0.001) × (Slope/100) + 0.001. Meanwhile, the Compound Topographic Index (CTI) assesses the hydrological characteristics of a landscape by identifying areas prone to water saturation based on the contributing upstream area and the local slope gradient. This index is calculated using the expression: CTI = ln((Flow Accumulation + 0.001)/((Slope/100)/0.001)). These parameters, the erosion vulnerability map, is created to spatially identify the areas of erosion and deposition.

3. RESULTS AND DISCUSSIONS

3.1 River Network Characteristics

Sampling was conducted during July (Sampling 1) and September (Sampling 2) to capture the variations in the transported sediments. Field observations revealed angular, low-sphericity boulders along the riverbanks and rounded, high-sphericity sediments on the riverbeds, indicating variations in transport history and depositional environment. Notably, wake regions, where turbulent flow forms behind large boulders, were identified, affecting the energy dynamics of the stream [12].

3.2 Sediment Classification and Distribution

The graphical representation of the Particle Size Distribution (PSD) curve, with the x-axis showing particle sizes on a logarithmic scale and the y-axis representing cumulative passing percentages. The distribution curves reveal differences in sediment sorting and grain size across sampling points. In July, sediments were more uniformly distributed, with finer particles prevalent in left-bank samples (SP1-LB) and coarser materials in the center (SP1-C) and confluence areas (SP2-C, SP2-Con). Histograms indicate multimodal distributions (bimodal or trimodal), suggesting a mixture of fine, medium, and coarse sediments, highlighting fluctuating flow energy [8,13,14].

In contrast, the September samples displayed steeper PSD curves at smaller grain sizes, indicative of finer particles and poorer sorting. Sampling points showed distinct distributions, with flatter curves in the river's center suggesting mixed energy transport and deposition. The samples reflected wider grain size variation, while the September samples were dominated mostly by sand. Histograms and PSD curves align with the reference study [15], showing similar descriptions for sorting, skewness, and kurtosis across samples. The sieve analysis also indicates that the sediment characteristics are heavily influenced by the watershed's lithology, stream behavior, flow energy, and climatic variations [14,16,17].

3.3 River Cross-Sectional Profile from Discharge Point to Upstream

The sampling Point 1 features a wide channel and a low average velocity of 0.08462 m/s, resulting in a relatively high discharge of 0.7706 m^3/s. These characteristics support a depositional environment, where fine sediments tend to accumulate due to limited transport capacity. In contrast, Sampling Point 2 has a narrower cross-section (0.7338 m^2) and a significantly higher average velocity of 0.55556 m/s. The discharge is lower at 0.40995 m^3/s, but the increased velocity enhances the stream's ability to transport fine to very-fine gravel materials [8,9], indicative of a more dynamic and erosive fluvial setting. Sampling Point 4 presents a wide cross-sectional area (10.5330 m^2) and a moderate flow velocity of 0.23333 m/s. It registers the highest discharge among the three at 2.7092 m^3/s. These conditions are conducive to the deposition of sandy fine gravel, suggesting a transitional zone between sediment transport and accumulation [3,18,19].

3.4 Hjulstrom Diagram

Based on the plotted samples (SP1 to SP9), SP1 and SP 3 fall within the deposition zone, indicating settling, while SP2, SP8, and SP9 are in the erosion and transport zones; the SP4 and SP7 suggest active movement under current flow conditions (Fig. 5).

3.5 Moments Method

During the July sampling, kurtosis values ranged from 1.880 to 9.647, indicating a platykurtic to very leptokurtic distribution, with an average of 3.621, suggesting a generally mesokurtic character. One sample showed a very leptokurtic yet poorly sorted distribution, aligning with its location in a narrow, high-flow river section [8]. This pattern reflects the interplay of steady sediment transport and abrupt inputs typical in confined

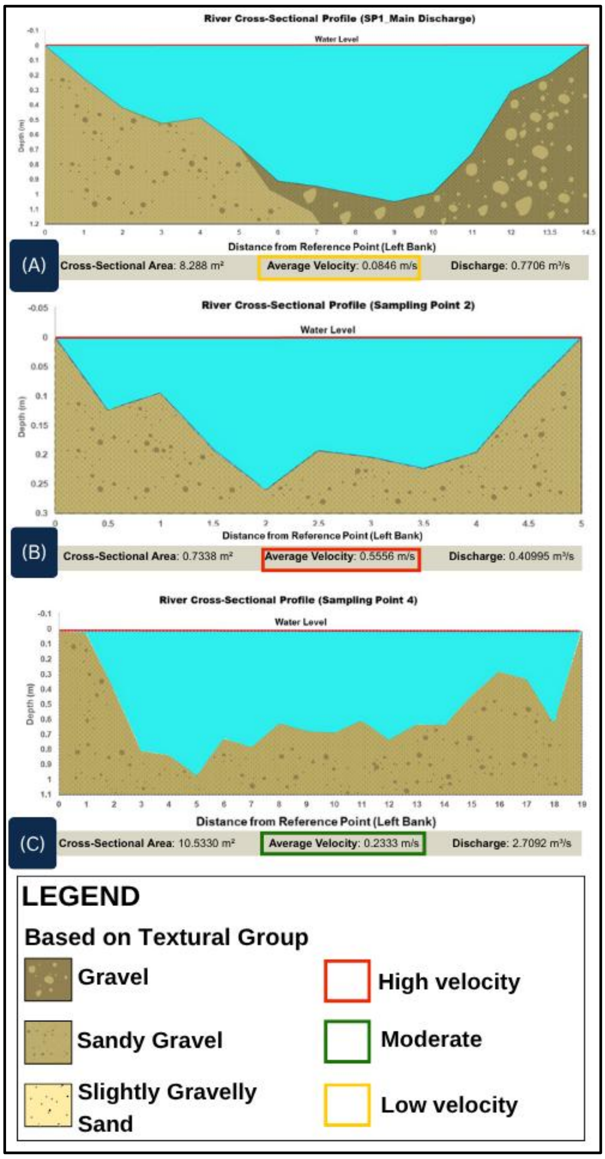

Fig 4. Representative River Cross-Sectional Profile from Discharge Point to Upstream.

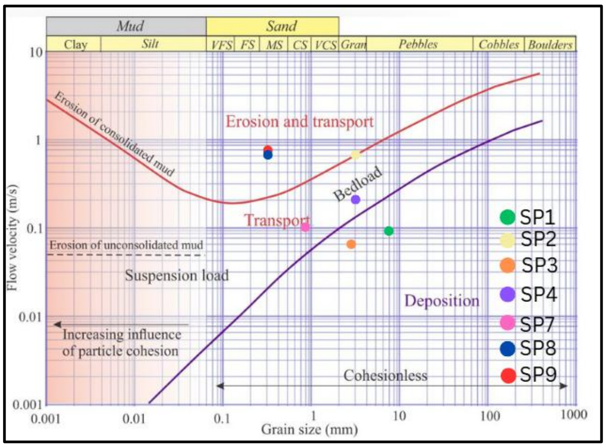

Fig 5. Hjulstrom Diagram Plotted value from sediment sizes and average water velocity

fluvial channels. Skewness during this period ranged from -0.231 to 1.826 (coarse to very fine skewed), averaging 0.379, indicating symmetrical to fine-grained dominance, with negative values corresponding to coarser deposits [15].

Notably, an increase in skewness was associated with an increase in kurtosis, highlighting a negative relationship. In contrast, during the September sampling, kurtosis values ranged from 2.064 to 5.220 (platykurtic to leptokurtic), with an average of 2.893, also reflecting a mesokurtic character. Skewness values spanned -0.669 to 1.397, averaging 0.474, indicating a slightly finer skewed nature (Table 4). This likewise displayed a negative relationship between skewness and kurtosis, mirroring the July conditions (see Table 3). These variations suggest a dynamic fluvial setting in Manoligao, where finer materials are selectively retained or introduced post-deposition, consistent with findings on fluvial sediment behavior [9].

Table 3. Summary of Kurtosis and Skewness in Different Sampling Points (July Samples)

SP	Skewness (Interpretation)	Kurtosis (Interpretation)
SP1-LB	0.113 (Coarse skewed)	1.974 (Platykurtic)
SP1-RB	0.305 (Symmetrical)	2.145 (Platykurtic)
SP1-C	-0.231 (Coarse skewed)	1.880 (Platykurtic)
SP2-C	0.110 (Fine skewed)	2.457 (Platykurtic)
SP2-CON	1.826 (Very fine skewed)	9.647 (Very leptokurtic)

Table 4. Summary of Kurtosis and Skewness in Different Sampling Points (September Samples)

SP	Skewness (Interpretation)	Kurtosis (Interpretation)
SP-LB	0.494 (Fine skewed)	3.390 (Mesokurtic)
SP-1RB	0.361 (Very fine skewed)	5.323 (Platykurtic
SP-1C	0.331 (Symmetrical)	2.430 (Platykurtic)
SP2-LB	0.319 (Symmetrical)	2.229 (Platykurtic)
SP2-RB	0.284 (Symmetrical)	2.206(Platykurtic)
SP2-C	0.378 (Symmetrical)	2.565 (Mesokurtic)
SP3-LB	0.267(Symmetrical)	2.351 (Platykurtic)
SP3-RB	0.512(Fine skewed)	2.852 (Mesokurtic)
SP3-C	0.525(Fine skewed)	2.712 (Mesokurtic)
SP4-RB	0.706(Fine skewed)	2.911(Mesokurtic)
SP4-C	0.816 (Fine skewed)	3.762 (Leptokurtic)
SP6-RB	-0.211 (Coarse skewed)	3.762 (Leptokurtic)
SP7-LB	-0.669 (Coarse skewed)	2.985 (Mesokurtic)
SP8-LB	0.652 (Fine skewed)	2.892 (Mesokurtic)
SP8-C	0.713 (Fine skewed)	2.905 (Mesokurtic)
SP9-LB	0.733 (Fine skewed)	2.504 (Platykurtic)
SP9-RB	1.397 (Very fine skewed)	5.220 (Leptokurtic)
SP9-C	1.092 (Fine skewed)	3.400 (Mesokurtic)
SP10-TB	0.039 (Symmetrical)	2.064 (Platykurtic)

3.6 Sediment Budget

Corporating the results from the field observations, grain size analysis of riverbed sediments, the transport condition of the watershed, and the calculated total suspended sediments (TSS) gives insights into the erodibility rate categorization. Based on the calculated data the SSC systematically increased with Q as well as the SSL, SSY and Sediment Budget (i.e., Sampling 3 and

4), but gathered data is not enough to conclude, since based on the study of Domingo et al. [6], they sampled suspended sediments once every 7 days in the dry season, once every 3 days in the wet season, and daily during prolonged rainfall (e.g., typhoon events). Table 5 summarizes the sediment budget and erosion rate calculation using suspended sediments. Despite that, climatic conditions are the main factor. Another factor is the river morphology (i.e., point bar); sampling point 3 is in the depositional zone (based on field observations). The upstream zone of the watershed (see Fig. 6) is dominated by the depositional environment, which shifts to erosional in sampling point 4 and continues depositional settings until the discharge point. The shift of the erosional environment in sampling point 4 is due to river morphology.

Table 5. Calculation of Sediment Budget and Erosion Rate Using the Suspended Sediment Concentration

SP	A	Q	SC	SL	SY	ER	SB
1	1.0035	0.771	0.1	0.0771	0.078	0.098	-1.4453
3	2.1461	0.708	2.15	1.5223	0.709	0.908	-0.6607
4	2.1461	2.079	1.05	2.1832	1.017	1.303	2.1094
7	2.1461	0.738	0.1	0.0738	0.034	0.044	-0.0472
8	2.1461	1.751	0.1	0.1760	0.082	0.104	-0.0009

SP=Sampling Point, A=Area,Q=Discharge, SC=Sediment Concentration, SL= Sediment Load, SY=Sediment Yield, SB=Sediment Budget

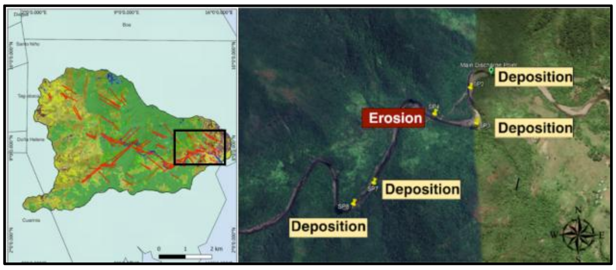

Fig.6 The Sediment Transport of Manoligao watershed Based on the Sediment Budget Calculation from the Suspended Sediment Concentrations.

3.7 Spatial Analysis

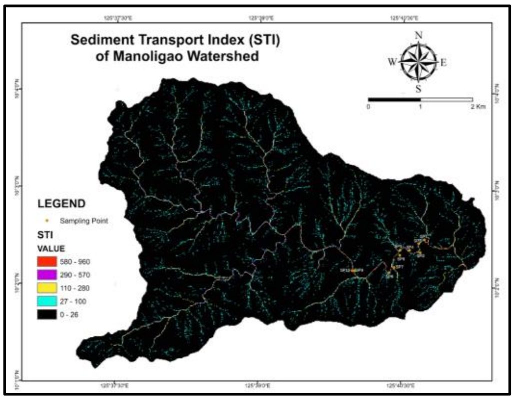

Fig 7. Sediment Transport Index Map

Several factors control sediment transportation within the catchment or watersheds, including gravity, slopes, and rainfall concentration [20,21,22,23]. The highest sediment transport index (STI) values (e.g., 117.47), which are associated with steep slopes and ridges, where erosion and sediment movement were most intense [24]. Conversely, the lowest STI values reflect slow sediment mobility and accumulation [25].

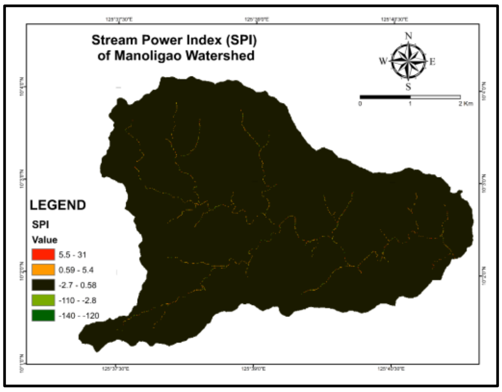

Fig 8. Stream Power Index Map

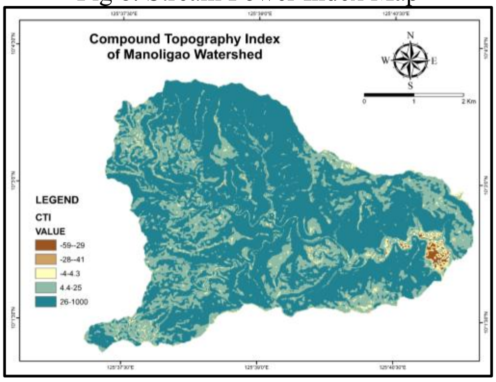

Fig 9. Compound Topography Index Map

In the case of the Manoligao watershed, high STI values represented yellow-red zones (e.g., SP2, SP4, SP5, SP7, SP8, and SP9), indicating significant erosion due to steep slopes (i.e., observed during field observation). In contrast, low STI values are represented by black and blue zones (e.g., SP1, SP3, SP6, and SP10), reducing water velocity and allowing sediment to settle (i.e., evident using field data), were associated with gentle slopes and areas of sediment accumulation (Fig. 7).
Additionally, high erosion is commonly observed along the main river, where water flow is most concentrated, causing intense sediment transport and channel erosion. Likewise, in this study, the erosion is still significant in downstream areas, suggesting that Manoligao maintains a high energy level, likely due to steep gradients that accelerate water velocity. The Stream Power Index (SPI) (Fig. 8) is a secondary topographic attribute derived from the flow accumulation and slope of an area. It quantifies the river channel's erosive power and indicates the topographic potential for sediment deposition in zones with low or negative values, while positive values signify areas prone to erosion. The CTI is a metric used to evaluate the hydrological characteristics of an area. The areas with a high potential for water saturation are based on the contributing upstream area and the local slope gradient in the watershed. Areas with high values are more prone to inundation, while low values are linked to steep slopes and channel systems. Intermediate values indicate regions vulnerable to land degradation and erosion. Flat and low-lying areas are especially at risk of sediment erosion and flooding due to water accumulation along slope gradients (see Fig. 9).
Structural control, particularly in tectonically active areas, plays a vital role in landscapes' erosional and morphological evolution [26]. In this study, the correlation between land cover and land use with erosion vulnerability indicates that closed forest distribution significantly influences the erodibility of the fluvial network. In contrast, shrub and open forests show low to

moderate effects on erosion. Additionally, the geology of Manoligao, characterized by highly jointed bedrock, contributes to its high susceptibility to erosion (Fig. 10).

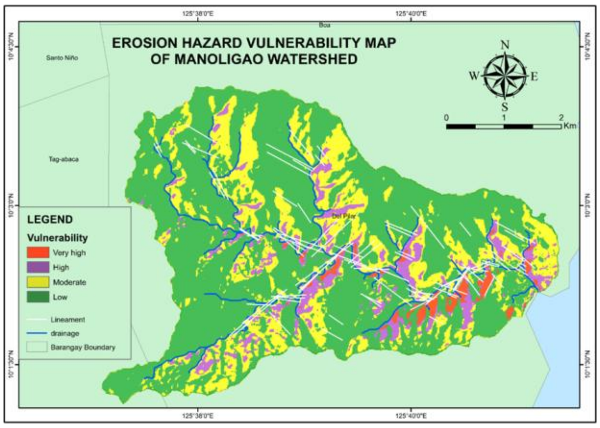

Fig 10. Erosion Hazard Vulnerability Map of Manoligao Watershed.

3.7 Evaluation of Results Based on Different Methodologies

Table 6 summarizes erosion and deposition zones identified using multiple methodologies, including sediment budget analysis, Hjulstrom diagrams, and hydrologic indices. It compares each sampling point's sediment status, transport conditions, and erosion vulnerability. The table highlights areas of consistent deposition or erosion, noting key hydrologic and geomorphic factors influencing these patterns.

4. CONCLUSION

The sediment transport dynamics of the Manoligao River are characterized by poorly sorted sand to gravel-sized particles, influenced by the proximity of ultramafic terrain. Riverbank sediments are angular with low sphericity, indicating minimal transport and closeness to the source, while riverbed sediments are more rounded due to longer transport through rolling and saltation. These characteristics reflect varying energy conditions, with extreme kurtosis suggesting high-energy sorting before deposition and positive skewness indicating the occasional settling of finer particles during calmer flows. The use of multiple methods, including Sediment Budget Calculation, Hjulstrom Diagram, Sediment Transport Index (STI), and Erosion Vulnerability Mapping, allowed for the identification of key erosion and deposition zones. SP1 and SP3 were consistently mapped as deposition areas, while SP2, SP4, and SP8 were associated with active erosion due to steep slopes and high-energy flow. SP7 and SP9 exhibited alternating behavior, highlighting local hydrodynamic variability. Each method contributed unique insights. Field-based sediment budgeting quantified transport rates but was constrained by the absence of fines. The Hjulstrom Diagram provided a useful visual framework, though it lacked detail on flow complexity. STI and erosion vulnerability mapping offered spatial insights but required validation specific to ultramafic geology.

5. RECOMMENDATIONS

This baseline study provides essential data to support the initiation of watershed conservation planning in the Municipality of Cagdianao. The use of GIS and remote sensing is recommended to establish monitoring systems and guide sediment management strategies. Collaboration among local government units, NGOs, and academic institutions is encouraged to facilitate data collection, build technical capacity, and support community-based water quality efforts. Engineering interventions such as gabion walls and riprap linings are suggested to stabilize eroding riverbanks, while bioengineering approaches offer ecological and structural advantages, especially within ultramafic terrains [3,7,26]. Although dam construction was not assessed, the study's findings can inform future hydrologic and geotechnical feasibility evaluations. Given the absence of fine sediments, suspended sediment budgeting using TSS data is suitable. Future studies should prioritize regular monitoring, sediment transport modeling, and engineering-focused research. The Hjulstrom Diagram remains applicable for evaluating sediment thresholds, while STI and erosion vulnerability mapping can provide spatial understanding if guided by detailed geological reconnaissance.

Table 6. Identification of zones of erosion and deposition.

	Sediment Budget Calculation	**Hjulstrom Diagram**	**Hydrologic Indices** (STI, SPI and CTI)	**Erosion Vulnerability** (Very High, High, Moderate and Low)	**Remarks**
SP 1	Deposition	Deposition	Deposition	Moderate to Low	Consistent deposition across all methods.
SP 2	Deposition	Erosion	Erosion	Very High to High	The deposition in the suspended budget is attributed to a lower discharge, which implies temporary sediment buildup. The narrow river and high flow energy keep erosion ongoing, as indicated by Hjulstrom, STI, and erosion vulnerability
SP 3	Deposition	Deposition	Deposition	Very High to High	Erosion vulnerability suggests potential for erosion, but all methods point to deposition due to reduced flow and a wider channel, which corresponds with the river's morphology (i.e. point bar).

SP 4	Erosion	Transport	Erosion	High to Moderate	All methods indicate active sediment movement and erosion, corresponding with the river's morphology (i.e. cut bank), high sediment yield, and water flow.
SP 5	-	-	Erosion	High to Moderate	Not classified in the Sediment Budget or Hjulstrom (no samples gathered), but STI and erosion vulnerability mapping suggest erosion is associated with the extensive joint structure.
SP 6	-	-	Deposition	Very High to High	Based on the STI and erosion vulnerability, it is classified as erosion, particularly in relation to the extensive joint structure located near sampling point 5.
SP 7	Deposition	Transport	Erosion	Very High	Deposition occurs during low flow and low sediment yield, while other methods suggest erosion, which is associated with a highly jointed structure. This suggests that active erosion takes place during peak discharge, as indicated by the field data showing a high discharge value.
SP 8	Deposition	Erosion	Erosion	Very High	The suspended budget shows deposition due to low sediment yield despite high water flow. In contrast, other methods suggest that erosion occurs, which may imply localized settling with predominant erosion forces during high flow events. Additionally, the area appears to be highly jointed.
SP 9	-	Erosion	Erosion	Moderate to Low	Erosion is significant in this area, likely due to steep slope, high water flow, and high discharge, according to the field data
SP 10	-	-	Deposition	Moderate to Low	Consistently identified as a deposition zone.

7. REFERENCES

[1] B. Zeiringer, C. Seliger, F. Greimel, and S. Schmutz, "River hydrology, flow alteration, and environmental flow," in Springer eBooks, pp. 67–89, (2018). https://doi.org/10.1007/978-3-319-73250

[2] M. Pidwirny, "Erosion and Deposition," Fundamentals of Physical Geography, 2nd ed., 2006. [Online]. Available:http://www.physicalgeography.net/fundamentals/10w.html

[3] R. D. M. Cabahug and A. J. Villanueva, "Assessment of soil erosion, sediment transport and deposition along Cagayan de Oro River," Mindanao Journal of Science and Technology, vol. 12, pp. 5–20, (2014). [Online]. Available: https://mjst.ustp.edu.ph/index.php/mjst/article/view/42

[4] Philippine Atmospheric, Geophysical and Astronomical Services Administration, "Climate of the Philippines," n.d. [Online]. Available: https://www.pagasa.dost.gov.ph/information/climate-philippines

[5] Philippine Climate Change Assessment Working Group II, "Philippine climate change assessment: Working Group II – Impacts, vulnerabilities and adaptation," n.d. [Online]. Available: https://www.omlopezcenter.org/the-philippine-climate-change-assessmen

[6] M. Makinano-Santillan, M. V. Japitana, A. C. Gagula, S. M. S. Albores, J. R. C. Bautista, M. R. Llesis, and J. R. Santillan, "Land-cover characterization and water quality assessment of the Sambunotan Watershed, Dinagat Islands in support of the development of the watershed management plan," in Proc. Int. Exchange Innov. Conf. Eng. Sci. (IEICES), vol. 10, pp. 910–915, Oct. 17, (2024). https://doi.org/10.5109/7323368

[7] M. Makinano-Santillan, A. C. Gagula, S. M. Salcedo-Albores, J. L. E. Gesta, N. A. Pacle, R. K. P. Varela, and J. R. Santillan, "Combined hydrological and geologic assessment for sustainable management of the Sambunotan Watershed, Dinagat Islands, Philippines," in Proc. Int. Exchange Innov. Conf. Eng. Sci. (IEICES), vol. 10, pp. [pages], (2024). https://doi.org/10.5109/7323375

[8] X. Zexing, Z. Chenling, Y. Qiang, W. Xiekang, and Y. Xufeng, "Hydrodynamics and bed morphological characteristics around a boulder in a gravel stream," Water Science & Technology Water Supply, vol. 20, no. 2, pp. 395–407, (2019).

[9] S. J. Blott and K. Pye, "GRADISTAT: A grain size distribution and statistics package for the analysis of unconsolidated sediments," Earth Surface Processes and Landforms, vol. 26, no. 11, pp. 1237–1248, (2011.https://doi.org/10.1002/esp.261

[10] R. L. Folk and W. C. Ward, "Brazos River bar: A study in the significance of grain size parameters," Journal of Sedimentary Research, vol. 27, no. 1, pp. 3–26, (1967): https://doi.org/10.1306/74d70646-2b21-11d7-8648000102c1865d

[11] J. P. T. Domingo, M. Attal, S. M. Mudd, B. T. Ngwenya, and C. P. C. David, "Seasonal fluxes and sediment routing in tropical catchments affected by nickel mining," Earth Surface Processes and Landforms, vol. 46, no. 13, pp. 2632–2655, (2021). https://doi.org/10.1002/esp.5198

[12] L. A. James, "Sustained reworking of hydraulic mining sediment in California: G. K. Gilbert's sediment wave model reconsidered," Zeitschrift für Geomorphologie, N. F., Suppl.-Bd. 88, pp. 49–66, (1993)..

[13] H. Cheng, J. He, X. Zou, J. Li, C. Liu, B. Liu, C. Zhang, Y. Wu, and L. Kang, "Characteristics of particle size for creeping and saltating sand grains in aeolian transport," Sedimentology, vol. 62, no. 5, pp. 1497–1511,(2015).https://doi.org/10.1111/sed.12191

[14] W. R. Muttashar, L. S. Bryson, and Z. A. Al-Humaidan, "The use of particle size distribution integrated with consistency limits for experimentally simulating fine-grained sedimentary units," Arabian Journal of Geosciences, vol. 14, no. 22, (2021). https://doi.org/10.1007/s12517-021-08812-7

[15] B. Otunola and K. Liu, "Granulometric and depositional characteristics of sandstones from Knysna and Robberg Formations, South Africa," Journal of Engineering and Applied Sciences, vol. 14, pp. 114–123, (2019).

[16] A. Van B Weaver and A. W. Stone, "Distinguishing sub-environments of sediment deposition in reservoirs using particle size distribution parameters," Journal of the Limnological Society of Southern Africa, vol. 6, no. 1, pp. 59–65, (1980): https://doi.org/10.1080/03779688.1980.9633210

[17] D. A. Edmonds and R. L. Slingerland, "Significant effect of sediment cohesion on delta morphology," Nature Geoscience, vol. 3, no. 2, pp. 105–109, (2009).https://doi.org/10.1038/ngeo730

[18] H. Chanson, Hydraulics of Open Channel Flow: An Introduction, 2nd ed. Oxford, U.K.: Elsevier, 2004.

[19] V. T. Chow, Open-Channel Hydraulics. New York, NY, USA: McGraw-Hill, (1959).

[20] R. Li, L. Xiong, B. Xiong, Y. Li, Q. Xu, L. Cheng, and C. Xu, "Investigating the downstream sediment load change by an index coupling effective rainfall information with reservoir sediment trapping capacity," Journal of Hydrology, vol. 590, 125200, (2020).https://doi.org/10.1016/j.jhydrol.2020.125200

[21] C. M. Casserly, J. N. Turner, J. J. O. Sullivan, M. Bruen, C. Bullock, S. Atkinson, and M. Kelly-Quinn, "Effect of low-head dams on reach-scale suspended sediment dynamics in coarse-bedded streams," Journal of Environmental Management, vol. 277, 111452,(2021).https://doi.org/10.1016/j.jenvman.2020.111452

[22] F. Zhang, M. Wang, and M. Yang, "Successful application of the Taguchi method to simulated soil erosion experiments at the slope scale under various conditions," CATENA, vol. 196, 104835, (2021).

[23] K. Zhu, Z. Li, L. Duan, Y. Li, and X. Xu, "Multiscale relationships between monthly sediment load and pertinent factors in a typical karst mountainous watershed," Journal of Hydrology, vol. 607, 127474, (2022).https://doi.org/10.1016/j.jhydrol.2022.127474

[24] S. A. A. El-Magd, H. O. Orabi, S. A. Ali, F. Parvin, and Q. B. Pham, "An integrated approach for evaluating the flash flood risk and potential erosion using the hydrologic indices and morpho-tectonic parameters," Environmental Earth Sciences, vol. 80, no. 20, (2021). https://doi.org/10.1007/s12665-021-10013-0

[25] N. Ennaji, O. Hasan, H. Said, and A. Mohamed, "Sediment Transport Index (STI) modeling using the GIS at small agricultural catchment," International Journal of Novel Research in Engineering & Pharmaceutical Sciences, vol. 2, no. 11, (2022). Available: ISSN: 2583-1658

[26] M. Moldovan, I. Tăut, F. A. Rebrean, B. Szilard, I. D. Arion, and M. Dîrja, "Determining the Anti-Erosion efficiency of forest stands installed on degraded land," Sustainability, vol. 14, no. 23, p. 15727, (2022). https://doi.org/10.3390/su142315727